Research article

Caffeine causes cell cycle arrest at G0/G1 and increases of ubiquitinated proteins, ATP and mitochondrial membrane potential in renal cells

Rattiyaporn Kanlaya, Chonnicha Subkod, Supanan Nanthawuttiphan, Visith Thongboonkerd [*]

Medical Proteomics Unit, Research Department, Faculty of Medicine Siriraj Hospital, Mahidol University, Bangkok, Thailand

A B S T R A C T

Caffeine is a well-known purine alkaloid commonly found in coffee. Several lines of previous and recent evidence have shown that habitual coffee drinking is associated with lower risks for chronic kidney disease (CKD) and nephrolithiasis. However, cellular and molecular mechanisms underlying its renoprotective effects remain largely unknown due to a lack of knowledge on cellular adaptive response to caffeine. This study investigated cellular adaptive response of renal tubular cells to caffeine at the protein level. Cellular proteome of MDCK cells treated with caffeine at a physiologic concentration (100 μM) for 24 h was analyzed comparing with that of untreated cells by label-free quantitative proteomics. From a total of 936 proteins identified, comparative analysis revealed significant changes in levels of 148 proteins induced by caffeine. These significantly altered proteins were involved mainly in proteasome, ribosome, tricarboxylic acid (TCA) (or Krebs) cycle, DNA replication, spliceosome, biosynthesis of amino acid, carbon metabolism, nucleocytoplasmic transport, cell cycle, cytoplasmic translation, translation initiation, and mRNA metabolic process. Functional validation by various assays confirmed that caffeine decreased cell population at G2/M, increased cell population at G0/G1, increased level of ubiquitinated proteins, increased intracellular ATP and enhanced mitochondrial membrane potential in MDCK cells. These data may help unravelling molecular mechanisms underlying the biological effects of caffeine on renal tubular cells at cellular and protein levels.

1. Introduction

Caffeine (1,3,7- trimethylxanthine) is a purine alkaloid commonly found in coffee. It is also found in other foods and beverages, e.g., guarana berries, cocoa, energy drinks, and soft drinks [1]. Accumulative data from different areas around the globe have suggested that moderate consumption of caffeine, i.e., 2.5 cups of coffee (containing approximately 200 mg of caffeine) at once or up to 5 cups of coffee (containing approximately 400 mg of caffeine) per day, is safe [2,3]. After 45 min of intake, caffeine is entirely absorbed by the gastrointestinal tract. Caffeine metabolism occurs in the liver by cytochrome (CYP) P450, which is responsible for metabolism of endogenous compounds and xenobiotics in human body [4]. Caffeine is metabolized mainly by CYP1A2 to four major metabolites, i.e., paraxanthine, theophylline, theobromine, and 1,3,7-trimethyluretic acid [4]. Since chemical structure of caffeine is similar to adenosine, it acts as an antagonist of all types of adenosine receptors, thereby affecting various systems throughout the body, including central nervous, digestive, immune,

musculoskeletal, circulatory and urinary systems [5].

Several lines of previous and recent studies have shown the beneficial effects of habitual caffeine and coffee consumption on human health under normal and disease states, particularly Type 2 diabetes, coronary heart disease, depression, obesity, neurodegenerative disorder, liver diseases, and cancers [1,6,7]. Recent systematic review and meta-analysis of clinical studies have revealed that coffee intake is associated with the lower incidence of CKD in a dose-dependent manner [8]. The association between coffee consumption and lower risk of CKD is also supported by other two studies [9,10]. In the context of kidney stone disease (nephrolithiasis), several lines of recent evidence have consistently shown the protective roles of caffeine against nephrolithiasis [11–15]. Although a previous study has demonstrated an acute effect of caffeine to increase urinary calcium excretion [16], such effect is likely to be encountered by its diuretic and natriuretic activities (independent of renal tubular Na^+/H^+ exchanger isoform 3 [17]), resulting in lower risk of nephrolithiasis [12].

Nevertheless, precise cellular and molecular mechanisms underlying

the effects of caffeine on renal tubular cells remain largely unknown. This study therefore investigated cellular adaptive response of renal tubular cells to caffeine at the protein level using a quantitative proteomics approach.

2. Materials and methods

2.1. Culture of renal tubular cells

MDCK renal tubular cells (ATCC; Manassas, VA) were grown in an MEM medium (Gibco; Grand Island, NY) supplemented with 10% heat-inactivated fetal bovine serum (Gibco), 60 U/ml penicillin G (Sigma-Aldrich; St. Louis, MO) and 60 µg/ml streptomycin (Sigma-Aldrich). The culture was done at 37 °C in a humidified incubator with 5% CO_2.

2.2. Defining the optimal concentration of caffeine for cell treatment

The cells were seeded into 6-well plate (approximately 5×10^5 cells/well). After 24-h incubation, the cells were treated with caffeine (Sigma-Aldrich) at 0.1, 1, 10, 100, or 1000 µM for 24 h. Thereafter, the cells were trypsinized, total cell number was counted, and cell death was determined by trypan blue exclusion assay. The blue-stained (dead) cells were counted and used for calculation of percentage of cell death as follows.

$$\% \text{ Cell death} = (\text{Number of dead cells} / \text{Total cell number}) \times 100 \qquad (1)$$

The optimal caffeine concentration was defined as the highest concentration that did not significantly affect total cell number and cell death (when compared with the untreated cells). Such optimal concentration (100 µM) was then used for all subsequent experiments.

2.3. In-solution tryptic digestion, nanoflow liquid chromatography coupled to tandem mass spectrometry (nanoLC-ESI-LTQ-Orbitrap MS/MS), and label-free quantitative proteomics

After 24-h incubation with or without 100 µM caffeine, cellular proteins were extracted with SDT lysis buffer (4% SDS, 100 mM DTT, and 100 mM Tris-HCl; pH7.6). Protein concentrations were measured using Bio-Rad protein assay (Bio-Rad; Milano, Italy) based on Bradford's method. An equal amount (30 µg) of total proteins from each sample was subjected to in-solution tryptic digestion as described previously [18, 19]. The digested peptides were then analyzed by nanoLC-ESI-LTQ-Orbitrap MS/MS as previously reported [20,21].

The raw MS/MS files were processed using MaxQuant (version 2.1.4.0) equipped with Andromeda search engine. Proteins were identified from the UniProtKB/Swiss-Prot mammalian database using the following parameters: carbamidomethylation at cysteine (C) as fixed modification; oxidation at methionine (M) as variable modification; trypsin as the digesting enzyme; only one missed cleavage was allowed; precursor mass tolerance was 4.5 ppm; fragment mass tolerance was 0.5 Da; and charge state ions = +2, + 3. The false discovery rate (FDR) cutoff was 1% at both peptide-spectrum match (PSM) and protein levels. Label-free quantification (LFQ) of proteins was performed by using the MaxQuant LFQ (MaxLFQ) algorithm with match-between-runs. The other MaxQuant settings were set at default as previously reported [22]. The proteins identified as contaminants and reverse hits (decoy) and those identified only by site modifications were excluded. The LFQ intensity, generated according to the MaxLFQ algorithm, was used for statistical comparison by unpaired Student's t-test. The proteins with $\geq$ 1.5-fold-change and *p*-value < 0.05 were considered as significantly altered proteins.

2.4. Confirmation of significantly altered proteins by Western blot analyses

After 24-h incubation with or without 100 µM caffeine, cellular proteins were extracted with Laemmli's buffer and protein concentrations were measured using Bio-Rad protein assay based on Bradford's method. An equal amount (30 µg) of total proteins from each sample was subjected to separation by 12% SDS-PAGE. The separated proteins were then electro-transferred onto nitrocellulose membranes, which were subsequently incubated with 5% skim milk in PBS at 25 °C for 1 h to prevent non-specific background. After washing with PBS, the membranes were incubated with each of the primary (mouse monoclonal) antibodies at 4 °C overnight. These include anti-GAPDH (1:2000), anti-β-catenin (1:1000), anti-annexin A1 (1:500), and anti-β-actin (1:1000) antibodies (all of them were purchased from Santa Cruz Biotechnology (Santa Cruz, CA) and diluted in 1% skim milk in PBS). After washing, the membranes were incubated with corresponding secondary antibody conjugated with horseradish peroxidase (Sigma-Aldrich; St. Louis, MO) (1:20,000 in 1% skim milk/PBS) at 25 °C for 1 h. The membranes were extensively washed with PBS followed by incubation with an enhanced chemiluminescence substrate (Thermo Fisher Scientific) and autoradiography. Intensities of protein bands were measured by using Image-Quant TL software (GE Healthcare; Uppsala, Sweden).

### 2.5. Functional enrichment analysis of significantly altered proteins

All of the significantly altered proteins induced by caffeine were subjected to functional enrichment analysis using ShinyGO tool (version 0.77) (*http://bioinformatics.sdstate.edu/go/*) and KEGG pathway database (*https://www.genome.jp/kegg/pathway.html*) to obtain the biological significance of these caffeine-induced altered proteins. *P*-values were derived from hypergeometric distribution and adjusted by using the false discovery rate (FDR) method with the cutoff value at 0.05. The correlation of significant biological processes was demonstrated by using a hierarchical clustering tree based on the number of proteins shared among them. The relevant biological pathways obtained were validated by various functional investigations as follows.

2.6. Flow cytometric analysis of cell cycle distribution

After 24-h incubation with or without 100 µM caffeine, the cells were subjected to flow cytometric analysis of cell cycle distribution as described previously [23,24]. Briefly, the cells were collected by trypsinization followed by centrifugation at 300 $\times g$ for 5 min. The cells were then fixed with ice-cold 70% ethanol and incubated on ice for 2 h. After another centrifugation at 300 $\times g$ for 5 min, the cell pellets were resuspended in a staining solution (3 µg/ml propidium iodide and 100 µg/ml RNase in 0.1% tritonX-100/PBS) and incubated at 37 °C in the dark for 30 min. The samples were then analyzed by BD Accuri™ C6 flow cytometer (BD Biosciences; San Jose, CA). Data acquisition was done from 10,000 cells per each sample. Percentage of cell population in different phases of cell cycle (G0/G1, S and G2/M) was analyzed by ModFit LT 5.0 software (Verity Software House; Topsham, ME).

2.7. Measurement of level of ubiquitin-conjugated proteins

After 24-h incubation with or without 100 µM caffeine, the level of ubiquitin-conjugated proteins was measured by Western blot analysis as described above but with rabbit anti-ubiquitin antibody (Santa Cruz Biotechnology) (1:500 in 1% skim milk/PBS) as the primary antibody and swine-anti-rabbit IgG conjugated with horseradish peroxidase (1:1000 in 1% skim milk/PBS) as the secondary antibody. Immunoreactive bands were detected by using the enhanced chemiluminescence and autoradiography as described above. Multiple bands of the ubiquitin-conjugated proteins were then subjected to intensity analysis using ImageQuant TL software (GE Healthcare).
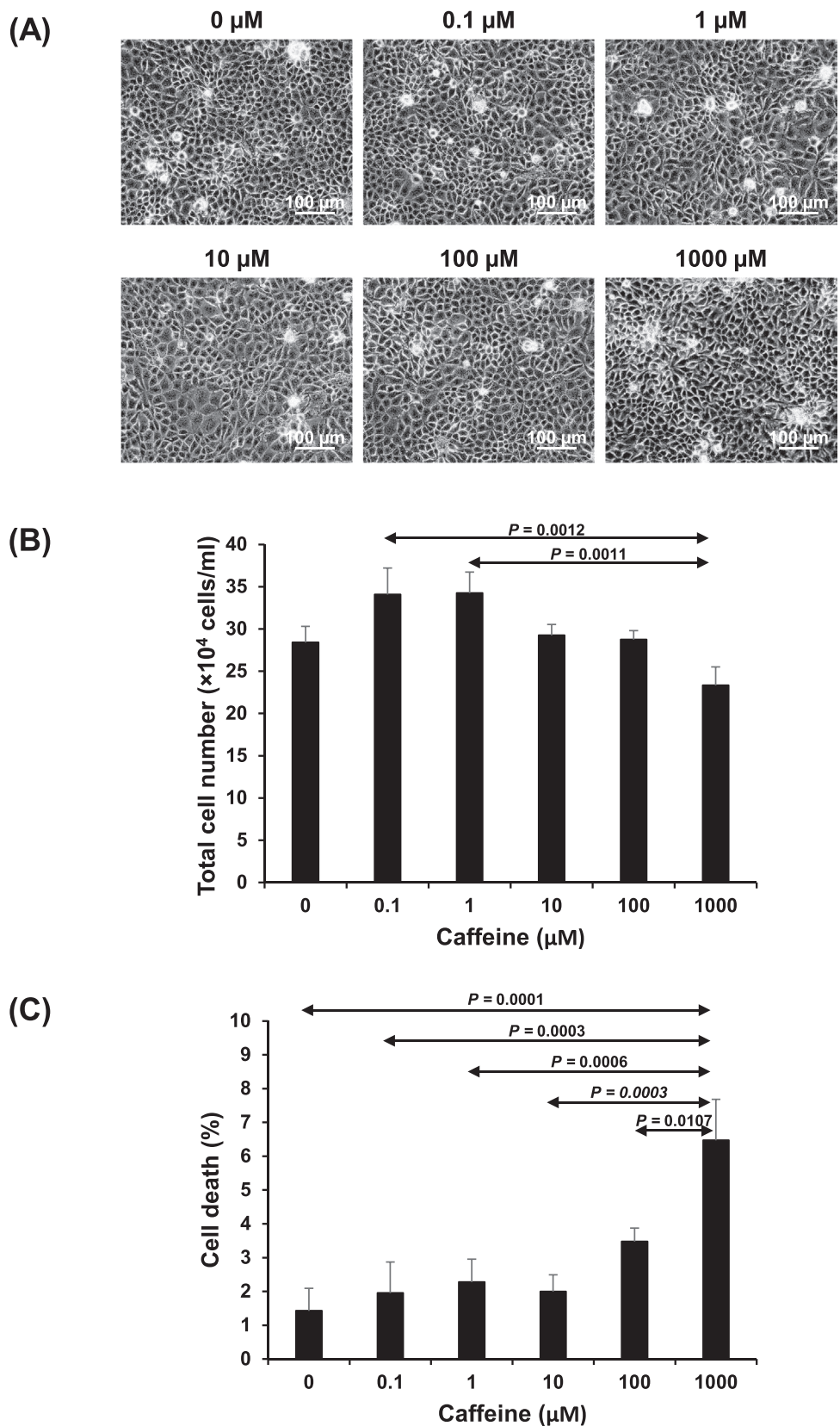
Fig. 1. Defining the optimal concentration of caffeine for cell treatment. (A): The cells were seeded into 6-well plate. After 24-h incubation, the cells were treated with caffeine at 0.1, 1, 10, 100, or 1000 μM for 24 h, whereas the untreated cells served as the control. (B and C): After trypsinization, total cell number was counted, and percentage of cell death was measured by trypan blue exclusion assay. The data are presented as mean ± SEM derived from three independent experiments using different biological samples. Only significant *p*-values are labelled.

Table 1
Summary of significantly altered proteins in renal tubular cells induced by caffeine treatment.

Protein name	Swiss-Prot ID	Gene Symbol	MS/MS identification Score	% Cov	No. of distinct/ total matched peptides	MW (kDa)	Intensity (× 10⁵ A.U.) Mean ± SEM		Ratio (Caffeine/ Control)	*P-value*
							Control	Caffeine		
14–3–3 protein gamma	P61983	*Ywhag*	223.6	55.1	9/13	28.3	33.01 ± 2.56	23.98 ± 2.05	0.73	0.0142
14–3–3 protein theta	Q3SZI4	*YWHAQ*	169.4	39.6	6/11	27.8	19.46 ± 1.81	13.69 ± 1.78	0.70	0.0370
26 S protease regulatory subunit 10B	P62335	*Psmc6*	90.0	36.8	11/11	44.2	19.60 ± 0.75	14.44 ± 1.41	0.74	0.0051
26 S protease regulatory subunit 6 A	P17980	*PSMC3*	69.4	24.4	8/8	49.2	16.36 ± 1.15	11.44 ± 1.25	0.70	0.0105
26 S proteasome non-ATPase regulatory subunit 1	Q3TXS7	*Psmd1*	51.9	9.2	4/4	105.7	15.20 ± 1.25	11.18 ± 0.85	0.74	0.0174
26 S proteasome non-ATPase regulatory subunit 5	Q0P5A6	*PSMD5*	20.5	6.8	3/3	56.0	7.53 ± 2.41	1.42 ± 0.98	0.19	0.0320
3'(2'),5'-bisphosphate nucleotidase 1	Q3ZCK3	*Bpnt1*	13.1	9.7	2/2	33.3	7.26 ± 0.98	2.74 ± 1.11	0.38	0.0076
40 S ribosomal protein S10	Q3T0F4	*Rps10*	49.7	33.3	5/5	18.9	68.42 ± 3.87	45.62 ± 4.75	0.67	0.0019
40 S ribosomal protein S11	Q3T0V4	*Rps11*	88.0	47.5	7/7	18.4	77.59 ± 5.61	50.41 ± 6.39	0.65	0.0056
40 S ribosomal protein S18	Q5TJE9	*Rps18*	115.4	52.6	10/10	17.7	50.76 ± 3.81	37.79 ± 4.45	0.74	0.0419
40 S ribosomal protein S24	Q56JU9	*Rps24*	40.3	29.8	4/4	15.2	32.65 ± 2.30	21.42 ± 1.86	0.66	0.0016
40 S ribosomal protein S27-like	Q3T0B7	*RPS27L*	30.9	25.0	2/2	9.5	83.21 ± 6.10	45.81 ± 5.13	0.55	0.0002
40 S ribosomal protein S29	P62276	*Rps29*	17.2	46.4	3/3	6.7	64.93 ± 5.45	45.78 ± 3.85	0.71	0.0112
40 S ribosomal protein S3a	Q56JV9	*RPS3A*	323.3	59.1	18/18	30.0	97.84 ± 7.72	68.89 ± 8.68	0.70	0.0240
60 S acidic ribosomal protein P0	P05388	*RPLP0*	225.3	45.4	11/11	34.3	81.53 ± 5.37	57.56 ± 5.17	0.71	0.0054
60 S ribosomal protein L14	Q3T0U2	*RPL14*	60.1	24.8	5/5	23.4	56.76 ± 3.64	38.42 ± 3.33	0.68	0.0019
60 S ribosomal protein L18	Q5E973	*RPL18*	102.4	34.0	6/6	21.5	92.64 ± 8.24	66.49 ± 6.10	0.72	0.0213
60 S ribosomal protein L21	P49666	*RPL21*	51.2	33.1	5/5	18.6	52.04 ± 4.34	25.64 ± 3.27	0.49	0.0002
60 S ribosomal protein L22	P67985	*Rpl22*	62.5	49.2	5/5	14.8	80.55 ± 7.69	56.44 ± 5.75	0.70	0.0231
60 S ribosomal protein L24	Q862I1	*Rpl24*	101.5	32.5	6/6	17.8	73.55 ± 4.61	53.91 ± 3.97	0.73	0.0053
60 S ribosomal protein L27a	Q56K03	*RPL27A*	25.1	23.6	3/3	16.6	87.87 ± 7.97	42.25 ± 10.80	0.48	0.0037
60 S ribosomal protein L35a	Q56JY1	*RPL35A*	31.8	26.4	3/3	12.6	10.14 ± 2.07	2.48 ± 1.67	0.25	0.0109
60 S ribosomal protein L36	Q3T171	*RPL36*	29.4	32.4	4/4	12.2	31.46 ± 2.03	23.52 ± 1.85	0.75	0.0107
60 S ribosomal protein L7a	P12970	*Rpl7a*	168.5	36.8	11/11	30.0	72.40 ± 5.08	48.86 ± 4.98	0.67	0.0044
Actin-related protein 2/3 complex subunit 2	Q3MHR7	*Arpc2*	18.2	10.7	3/3	34.4	3.73 ± 1.87	8.97 ± 1.27	2.41	0.0339
Acyl-CoA-binding protein	Q9TQX6	*DBI*	22.5	50.6	3/3	10.0	50.06 ± 5.80	31.29 ± 3.09	0.63	0.0114
Aldose reductase	P16116	*Akr1b1*	13.0	8.3	2/2	35.9	17.24 ± 2.41	8.43 ± 1.39	0.49	0.0060
Annexin A1	P04083	*ANXA1*	192.7	22.0	3/9	38.7	369.02 ± 15.46	274.22 ± 23.07	0.74	0.0036
Apoptosis inhibitor 5	O35841	*Api5*	20.3	9.1	3/3	56.8	8.05 ± 0.69	2.65 ± 1.45	0.33	0.0040
ATP-dependent 6-phosphofructo-kinase, platelet type	P47860	*Pfkp*	24.3	6.0	1/3	85.7	12.96 ± 0.99	0.00 ± 0.00	0.00	< 0.0001
Bifunctional purine biosynthesis protein PURH	O35567	*Atic*	55.8	12.0	2/6	64.2	11.06 ± 0.73	7.20 ± 1.17	0.65	0.0130
Calcyclin-binding protein	Q3T168	*CACYBP*	17.8	10.9	3/3	26.3	1.76 ± 1.76	9.29 ± 1.93	5.27	0.0109
Carbonic anhydrase 2	P00918	*CA2*	15.6	10.0	2/2	29.3	23.23 ± 1.52	13.14 ± 2.87	0.57	0.0068
Catenin beta-1	Q0VCX4	*Ctnnb1*	40.4	11.1	4/5	85.5	6.44 ± 0.65	4.12 ± 0.35	0.64	0.0061
Cathepsin D	Q4LAL9	*CTSD*	60.7	20.0	5/5	44.3	17.36 ± 1.75	11.78 ± 1.93	0.68	0.0477

Table 1 (*continued*)

Protein name	Swiss-Prot ID	Gene Symbol	MS/MS identification Score	% Cov	No. of distinct/ total matched peptides	MW (kDa)	Intensity (× 10^5 A.U.) Mean ± SEM		Ratio (Caffeine/ Control)	P-value
							Control	Caffeine		
Chloride intracellular channel protein 1	Q5E9B7	CLIC1	145.7	23.2	4/4	27.0	34.54 ± 1.93	25.52 ± 2.99	0.74	0.0220
Cleavage and polyadenylation specificity factor subunit 5	Q3ZCA2	Nudt21	24.2	18.5	4/4	26.2	6.12 ± 0.31	4.38 ± 0.40	0.72	0.0034
Coatomer subunit gamma-1	Q9QZE5	Copg1	85.0	15.6	10/10	97.5	11.19 ± 0.62	7.02 ± 1.16	0.63	0.0060
Cold shock domain-containing protein E1	O75534	CSDE1	80.1	18.0	13/13	88.9	13.67 ± 1.11	10.09 ± 0.93	0.74	0.0254
Core histone macro-H2A.1	Q02874	H2afy	7.5	5.7	1/1	39.5	16.82 ± 1.65	7.73 ± 2.54	0.46	0.0084
CTP synthase 1	P70698	Ctps1	25.4	8.3	4/4	66.7	8.39 ± 0.76	4.82 ± 1.49	0.58	0.0492
Cytochrome c oxidase subunit 5 A, mitochondrial	P00426	Cox5a	33.6	21.1	3/3	16.7	23.40 ± 2.26	14.61 ± 2.51	0.62	0.0192
Cytosolic non-specific dipeptidase	Q9D1A2	Cndp2	13.5	6.1	2/2	52.8	6.45 ± 0.96	2.52 ± 1.02	0.39	0.0124
Developmentally-regulated GTP-binding protein 1	Q3MHP5	DRG1	27.0	9.8	3/3	40.5	2.14 ± 0.70	3.97 ± 0.35	1.86	0.0316
Dihydropyrimidinase-related protein 2	O02675	Dpysl2	18.4	7.5	3/4	62.3	5.59 ± 0.76	2.87 ± 1.00	0.51	0.0457
DNA replication licensing factor MCM2	P49736	MCM2	34.2	5.1	1/4	101.9	5.53 ± 0.37	3.92 ± 0.56	0.71	0.0287
DNA replication licensing factor MCM3	A4FUD9	MCM3	60.4	12.7	9/9	90.9	7.86 ± 0.63	3.87 ± 1.58	0.49	0.0325
DNA replication licensing factor MCM6	Q2KIZ8	MCM6	25.1	8.3	4/4	92.9	5.12 ± 1.43	1.23 ± 0.90	0.24	0.0349
DNA-(apurinic or apyrimidinic site) lyase	P28352	Apex1	39.1	17.4	4/4	35.5	10.86 ± 0.49	7.61 ± 0.83	0.70	0.0037
DnaJ homolog subfamily A member 1	Q95JF4	DNAJA1	104.5	34.5	11/11	44.9	23.85 ± 1.82	16.23 ± 1.29	0.68	0.0035
Dolichyl-diphosphooligosaccharide–protein glycosyltransferase subunit 2	F1PCT7	RPN2	67.4	15.4	5/5	69.0	25.58 ± 1.62	18.22 ± 2.34	0.71	0.0199
Elongation factor 1-alpha 1	Q66RN5	EEF1A1	307.0	57.1	18/18	50.1	537.45 ± 26.17	384.51 ± 33.28	0.72	0.0023
Elongation factor 2	P13639	EEF2	323.3	44.4	32/33	95.3	134.05 ± 5.99	92.79 ± 9.42	0.69	0.0020
Eukaryotic initiation factor 4A-I	Q3SZ54	Eif4a1	323.3	54.2	15/17	46.2	173.34 ± 10.33	106.39 ± 10.78	0.61	0.0004
Eukaryotic initiation factor 4A-III	Q2NL22	Eif4a3	34.9	20.4	5/7	46.8	12.37 ± 1.66	7.33 ± 0.85	0.59	0.0158
Eukaryotic translation initiation factor 2 subunit 3	P81795	Eif2s3	108.5	23.9	8/8	51.1	31.30 ± 2.82	22.19 ± 1.87	0.71	0.0161
Eukaryotic translation initiation factor 3 subunit D	Q3T122	Eif3d	56.7	21.2	7/7	63.9	25.98 ± 2.26	17.98 ± 1.12	0.69	0.0060
Eukaryotic translation initiation factor 3 subunit E	Q3T102	Eif3e	53.9	14.8	6/6	52.2	13.88 ± 1.18	7.27 ± 0.95	0.52	0.0005
Eukaryotic translation initiation factor 3 subunit H	Q56JZ5	Eif3h	24.6	13.1	1/3	39.9	27.12 ± 1.71	18.39 ± 1.68	0.68	0.0022
Eukaryotic translation initiation factor 3 subunit K	Q3T0V3	EIF3K	34.7	16.1	3/3	25.1	18.88 ± 1.95	9.49 ± 2.49	0.50	0.0091
Eukaryotic translation initiation factor 4B	Q8BGD9	Eif4b	18.0	5.4	3/3	68.8	19.33 ± 2.01	14.16 ± 1.22	0.73	0.0428
Eukaryotic translation initiation factor 4 H	Q9WUK2	Eif4h	20.0	21.4	3/3	27.3	7.72 ± 2.06	1.82 ± 1.24	0.24	0.0262
Far upstream element-binding protein 1	Q32PX7	Fubp1	70.9	21.1	10/12	67.2	13.92 ± 1.18	10.15 ± 1.20	0.73	0.0394
Fumarate hydratase, mitochondrial	P07954	FH	20.3	6.3	2/2	54.6	0.98 ± 0.98	7.72 ± 1.57	7.91	0.0022
Glucose-6-phosphate isomerase	Q6P6V0	Gpi	9.7	2.7	1/1	62.8	1.11 ± 0.27	0.18 ± 0.09	0.16	0.0050
Glyceraldehyde-3-phosphate dehydrogenase	P10096	GAPDH	323.3	51.7	2/12	35.9	343.13 ± 18.66	241.24 ± 21.39	0.70	0.0025
Glycine–tRNA ligase	P41250	GARS	72.3	16.1	9/9	83.2	23.03 ± 1.40	16.26 ± 1.92	0.71	0.0115
Guanine nucleotide-binding protein G(I)/G(S)/G(T) subunit beta-1	P62871	Gnb1	38.4	24.1	6/6	37.4	10.42 ± 1.04	7.04 ± 1.07	0.68	0.0376
Guanine nucleotide-binding protein subunit beta-2-like 1	P63243	Gnb2l1	277.5	61.2	15/15	35.1	112.01 ± 10.05	75.58 ± 6.91	0.67	0.0087
Heterogeneous nuclear ribonucleoprotein F	Q5E9J1	Hnrnpf	174.1	21.0	4/6	45.7	24.95 ± 1.56	18.09 ± 1.90	0.72	0.0131

Table 1 (*continued*)

Protein name	Swiss-Prot ID	Gene Symbol	MS/MS identification Score	% Cov	No. of distinct/ total matched peptides	MW (kDa)	Intensity ($\times 10^5$ A.U.) Mean $\pm$ SEM		Ratio (Caffeine/ Control)	P-value
							Control	Caffeine		
Heterogeneous nuclear ribonucleoprotein H	P31943	HNRNPH1	323.3	27.8	7/9	49.2	68.58 $\pm$ 5.38	44.31 $\pm$ 4.76	0.65	0.0038
Heterogeneous nuclear ribonucleoprotein H3	P31942	HNRNPH3	36.4	11.3	3/3	36.9	4.60 $\pm$ 0.15	3.42 $\pm$ 0.34	0.74	0.0055
Heterogeneous nuclear ribonucleoprotein L	F1LQ48	Hnrnpl	73.1	20.1	9/9	67.9	24.87 $\pm$ 1.23	16.06 $\pm$ 1.50	0.65	0.0003
Heterogeneous nuclear ribonucleoprotein U	Q00839	HNRNPU	323.3	24.6	17/17	90.6	45.05 $\pm$ 2.21	30.82 $\pm$ 2.84	0.68	0.0011
Heterogeneous nuclear ribonucleoproteins A2/B1	O88569	Hnrnpa2b1	167.7	36.0	12/12	37.4	114.54 $\pm$ 9.33	84.60 $\pm$ 9.25	0.74	0.0367
High mobility group protein HMG-I/HMG-Y	P17096	HMGA1	13.2	10.3	2/2	11.7	5.67 $\pm$ 3.81	35.88 $\pm$ 9.64	6.32	0.0101
Histone H2B type 1-N	Q99877	HIST1H2BN	217.4	49.2	2/8	13.9	1155.00 $\pm$ 100.50	788.94 $\pm$ 95.01	0.68	0.0176
Histone H3.2	Q71DI3	HIST2H3A	11.0	44.1	1/6	15.4	2.45 $\pm$ 0.83	0.40 $\pm$ 0.20	0.16	0.0295
Importin subunit beta-1	P70168	Kpnb1	213.1	19.4	12/12	97.2	23.60 $\pm$ 1.47	17.65 $\pm$ 2.03	0.75	0.0303
Importin-5	Q8BKC5	Ipo5	314.8	23.2	18/18	123.6	20.57 $\pm$ 0.73	15.08 $\pm$ 1.38	0.73	0.0028
Interleukin enhancer-binding factor 3	Q12906	ILF3	80.5	15.4	8/8	95.3	14.47 $\pm$ 1.19	9.56 $\pm$ 0.99	0.66	0.0059
Keratin, type II cytoskeletal 8	P05786	KRT8	64.2	20.5	3/13	53.6	64.94 $\pm$ 6.88	26.85 $\pm$ 5.25	0.41	0.0004
Lamina-associated polypeptide 2, isoforms beta/delta/epsilon/ gamma	Q61029	Tmpo	36.3	12.6	5/5	50.4	17.57 $\pm$ 1.93	12.42 $\pm$ 1.43	0.71	0.0478
L-lactate dehydrogenase A chain	P19858	Ldha	84.9	26.5	5/10	36.6	106.82 $\pm$ 6.34	78.28 $\pm$ 7.90	0.73	0.0124
Lupus La protein	P10881	SSB	16.5	7.7	2/2	46.5	4.61 $\pm$ 0.45	3.11 $\pm$ 0.42	0.67	0.0271
Microtubule-associated protein RP/EB family member 1	Q15691	MAPRE1	38.8	32.8	6/6	30.0	18.54 $\pm$ 1.43	11.87 $\pm$ 2.73	0.64	0.0458
Mitochondrial import receptor subunit TOM70	Q75Q39	Tomm70a	12.2	3.3	1/2	67.4	5.47 $\pm$ 1.49	0.35 $\pm$ 0.35	0.06	0.0041
Myosin light polypeptide 6	P60661	Myl6	141.7	42.4	5/5	16.9	41.74 $\pm$ 3.64	30.52 $\pm$ 3.45	0.73	0.0398
N-alpha-acetyltransferase 15, NatA auxiliary subunit	Q9BXJ9	NAA15	27.0	5.5	4/4	101.3	8.25 $\pm$ 0.33	3.68 $\pm$ 1.19	0.45	0.0019
Neuroblast differentiation-associated protein AHNAK	Q09666	AHNAK	192.4	15.1	29/29	629.1	70.14 $\pm$ 4.23	51.51 $\pm$ 5.40	0.73	0.0152
Neutral alpha-glucosidase AB	Q8BHN3	Ganab	14.0	2.9	2/2	106.9	13.32 $\pm$ 1.14	7.77 $\pm$ 1.95	0.58	0.0255
NHP2-like protein 1	Q3B8S0	Nhp2l1	29.0	18.8	2/2	14.2	10.36 $\pm$ 2.32	1.23 $\pm$ 1.23	0.12	0.0031
Non-POU domain-containing octamer-binding protein	Q15233	NONO	91.7	27.8	10/11	54.2	25.78 $\pm$ 1.86	17.41 $\pm$ 2.06	0.68	0.0083
Non-specific lipid-transfer protein	P32020	Scp2	80.4	10.6	5/5	59.1	12.71 $\pm$ 0.95	7.26 $\pm$ 0.95	0.57	0.0009
Nuclear autoantigenic sperm protein	Q2T9P4	Nasp	42.5	8.4	4/4	83.7	12.50 $\pm$ 1.41	7.35 $\pm$ 1.53	0.59	0.0248
Nucleolar protein 56	O00567	NOP56	74.8	18.9	8/8	66.1	10.63 $\pm$ 0.55	7.24 $\pm$ 0.77	0.68	0.0025
Nucleolar protein 58	Q9Y2X3	NOP58	25.9	9.8	4/4	59.6	8.19 $\pm$ 0.87	5.25 $\pm$ 0.48	0.64	0.0091
Nucleolar RNA helicase 2	Q9NR30	DDX21	65.2	17.1	10/10	87.3	21.57 $\pm$ 1.37	15.92 $\pm$ 1.40	0.74	0.0108
Nucleophosmin	Q61937	Npm1	253.7	35.3	9/9	32.6	137.93 $\pm$ 7.31	103.06 $\pm$ 13.71	0.75	0.0393
Nucleoside diphosphate kinase B	Q3T0Q4	NME2	74.4	31.6	1/4	17.3	113.11 $\pm$ 10.03	79.66 $\pm$ 9.85	0.70	0.0302
Obg-like ATPase 1	A0JPJ7	Ola1	30.9	14.6	5/5	44.5	11.62 $\pm$ 1.43	6.41 $\pm$ 0.96	0.55	0.0082
Peptidyl-prolyl cis-trans isomerase FKBP1A	P26883	Fkbp1a	50.5	40.7	3/3	11.9	18.75 $\pm$ 1.32	9.59 $\pm$ 2.11	0.51	0.0020
Peroxiredoxin-1	Q06830	PRDX1	179.8	53.3	12/16	22.1	225.33 $\pm$ 15.55	163.65 $\pm$ 12.16	0.73	0.0065
Phosphoserine aminotransferase	Q9Y617	PSAT1	57.6	21.4	6/7	40.4	19.60 $\pm$ 1.47	14.26 $\pm$ 1.27	0.73	0.0142
Poly(rC)-binding protein 2	Q61990	Pcbp2	45.3	23.5	5/7	38.2	48.88 $\pm$ 1.68	35.19 $\pm$ 4.72	0.72	0.0147
Poly(U)-binding-splicing factor PUF60	Q2HJG2	PUF60	65.0	10.4	3/3	57.1	5.02 $\pm$ 1.75	10.01 $\pm$ 1.49	1.99	0.0457

Table 1 (*continued*)

Protein name	Swiss-Prot ID	Gene Symbol	MS/MS identification Score	% Cov	No. of distinct/ total matched peptides	MW (kDa)	Intensity ($\times 10^5$ A.U.) Mean ± SEM		Ratio (Caffeine/ Control)	*P-value*
							Control	Caffeine		
Polypyrimidine tract-binding protein 1	P26599	PTBP1	276.0	22.2	9/9	57.2	27.23 ± 1.86	19.88 ± 1.60	0.73	0.0086
Prefoldin subunit 2	A1A4P5	PFDN2	81.9	22.7	3/3	16.7	10.84 ± 0.74	7.37 ± 1.08	0.68	0.0173
Proteasome subunit alpha type-6	Q2YDE4	Psma6	47.9	26.4	6/6	27.4	29.21 ± 2.52	20.84 ± 2.22	0.71	0.0240
Proteasome subunit beta type-4	P99026	Psmb4	26.5	15.5	3/3	29.1	1.08 ± 1.08	6.43 ± 2.15	5.96	0.0411
Proteasome subunit beta type-5	O55234	Psmb5	57.6	15.2	3/3	28.5	12.80 ± 1.66	7.65 ± 1.41	0.60	0.0309
Protein arginine N-methyltransferase 1	Q63009	Prmt1	88.9	35.1	10/10	40.5	38.00 ± 3.96	25.41 ± 3.30	0.67	0.0266
Protein CYR61	P18406	Cyr61	12.4	30.6	2/9	41.7	30.01 ± 3.58	19.92 ± 2.77	0.66	0.0406
Protein S100-A10	Q6SQH4	S100A10	36.8	37.1	3/3	11.2	113.00 ± 14.89	63.84 ± 12.88	0.56	0.0238
Ran-specific GTPase-activating protein	P34022	Ranbp1	43.6	37.9	6/6	23.6	41.86 ± 2.32	30.85 ± 3.80	0.74	0.0251
Ras GTPase-activating protein-binding protein 1	Q32LC7	G3bp1	98.0	20.6	7/8	52.1	25.04 ± 1.39	17.40 ± 1.66	0.69	0.0028
Ras-related protein Rab-10	P61027	Rab10	44.7	20.5	3/4	22.5	15.81 ± 1.30	11.42 ± 1.30	0.72	0.0295
Ras-related protein Rab-11A	Q2TA29	Rab11a	38.2	25.9	5/5	24.5	17.46 ± 1.81	11.72 ± 1.85	0.67	0.0419
Ras-related protein Rab-1B	Q2HJH2	RAB1B	57.9	41.3	3/7	22.2	10.56 ± 0.60	7.31 ± 1.10	0.69	0.0193
Ras-related protein Rab-5B	P61021	Rab5b	62.2	23.7	3/4	23.7	10.54 ± 0.67	7.16 ± 0.87	0.68	0.0072
Ribonuclease inhibitor	Q91VI7	Rnh1	14.7	5.5	1/2	49.8	7.50 ± 1.49	2.67 ± 1.38	0.36	0.0302
Ribosomal protein L4	Q28346	RPL4	186.3	35.4	2/16	47.5	51.99 ± 4.43	30.44 ± 4.23	0.59	0.0028
S-adenosylmethionine synthase isoform type-2	Q3THS6	Mat2a	52.5	16.2	5/5	43.7	25.87 ± 1.19	19.09 ± 1.59	0.74	0.0035
Septin-7	Q9WVC0	SEPT7	29.8	10.8	3/4	50.5	14.03 ± 0.74	10.32 ± 0.98	0.74	0.0083
Serine/arginine-rich splicing factor 6	Q3TWW8	Srsf6	59.3	18.6	6/6	39.0	33.24 ± 3.28	23.70 ± 2.74	0.71	0.0403
Small nuclear ribonucleoprotein Sm D3	P62320	Snrpd3	15.1	15.1	2/2	13.9	33.53 ± 2.29	21.00 ± 2.40	0.63	0.0016
Small nuclear ribonucleoprotein-associated protein B	P27048	Snrpb	33.1	25.1	5/5	23.7	16.85 ± 1.49	10.64 ± 1.94	0.63	0.0217
Sorting nexin-6	Q9UNH7	SNX6	13.3	7.9	2/2	46.7	2.21 ± 0.74	0.32 ± 0.32	0.14	0.0312
Splicing factor 3B subunit 3	A0JN52	Sf3b3	27.8	2.1	2/2	135.6	9.18 ± 0.39	5.11 ± 1.33	0.56	0.0097
Succinyl-CoA ligase [ADP/GDP-forming] subunit alpha, mitochondrial	P13086	Suclg1	44.5	13.6	4/4	36.2	11.63 ± 1.28	7.33 ± 0.96	0.63	0.0159
Succinyl-CoA ligase [GDP-forming] subunit beta, mitochondrial	Q3MHX5	SUCLG2	46.3	5.8	2/2	46.7	0.50 ± 0.50	2.86 ± 0.76	5.73	0.0194
SUMO-activating enzyme subunit 1	A2VE14	SAE1	19.9	13.0	3/3	38.3	10.92 ± 0.67	6.88 ± 0.98	0.63	0.0037
T-complex protein 1 subunit delta	Q7TPB1	Cct4	184.4	38.2	17/17	58.1	48.15 ± 2.87	35.03 ± 3.63	0.73	0.0120
T-complex protein 1 subunit eta	Q2NKZ1	Cct7	323.3	50.8	1/24	59.4	61.85 ± 3.52	43.05 ± 3.09	0.70	0.0010
Thioredoxin	O97680	TXN	56.9	39.0	6/6	11.8	98.33 ± 8.74	67.48 ± 7.24	0.69	0.0152
Thioredoxin-dependent peroxide reductase, mitochondrial	P35705	PRDX3	69.5	14.4	3/3	28.2	11.43 ± 0.78	8.46 ± 0.83	0.74	0.0190
THO complex subunit 4	Q3T0I4	Alyref	39.4	32.3	5/5	27.0	22.82 ± 1.55	14.50 ± 3.16	0.64	0.0309
Transaldolase	Q9EQS0	Taldo1	29.6	13.1	4/4	37.5	20.87 ± 1.84	14.61 ± 1.75	0.70	0.0255
Transcription factor BTF3	Q64152	Btf3	47.0	37.3	4/4	22.0	44.84 ± 5.11	27.56 ± 2.52	0.61	0.0079
Transforming protein RhoA	P61585	Rhoa	31.0	18.1	2/4	21.8	26.18 ± 2.37	19.38 ± 1.46	0.74	0.0268
Transgelin-2	P37802	TAGLN2	323.3	81.9	17/17	22.4	126.59 ± 7.21	80.54 ± 7.92	0.64	0.0006

Table 1 (*continued*)

Protein name	Swiss-Prot ID	Gene Symbol	MS/MS identification Score	% Cov	No. of distinct/ total matched peptides	MW (kDa)	Intensity ($\times 10^5$ A.U.) Mean ± SEM		Ratio (Caffeine/ Control)	*P-value*
							Control	Caffeine		
Translationally-controlled tumor protein	A5A6K2	*TPT1*	61.8	32.6	6/6	19.6	48.92 ± 3.14	34.56 ± 4.45	0.71	0.0180
Tubulin beta-4B chain	Q3MHM5	*Tubb4b*	323.3	57.8	1/22	49.8	233.20 ± 13.93	167.63 ± 16.34	0.72	0.0076
Tubulin–tyrosine ligase-like protein 12	Q3UDE2	*Ttll12*	11.7	2.8	2/2	74.0	4.11 ± 1.14	0.90 ± 0.60	0.22	0.0239
Ubiquitin-40S ribosomal protein S27a	P62992	*RPS27A*	282.9	64.7	3/11	18.0	164.66 ± 13.96	114.75 ± 9.62	0.70	0.0095
UDP-glucose 6-dehydrogenase	O60701	*UGDH*	74.7	32.2	9/9	55.0	9.39 ± 0.55	6.61 ± 0.72	0.70	0.0074
Vinculin	P18206	*VCL*	160.4	19.8	2/17	123.8	28.39 ± 2.27	20.79 ± 2.32	0.73	0.0327
WD repeat-containing protein 1	O75083	*WDR1*	51.3	17.0	7/7	66.2	6.70 ± 1.09	0.00 ± 0.00	0.00	< 0.0001

A.U. = arbitrary unit; %Cov = percentage of sequence coverage.

2.8. Measurement of intracellular ATP level

After 24-h incubation with or without 100 μM caffeine, the cells were washed with PBS and then extracted by 100 μl ATP extraction buffer (25 mM Tricine, 100 μM EDTA, 1 mM DTT, and 1% Triton X-100). After centrifugation at 1000 $\times g$ at 4 °C for 5 min, the supernatant (extracted intracellular compartment) was collected for ATP measurement using the luminescence-based protocol [25,26]. The intracellular ATP level in each sample was determined from the standard curve, normalized by protein amount, and then reported as pmol/mg protein unit.

2.9. Quantitative analysis of mitochondrial membrane potential

The cells were seeded on coverslips at a density of 3.5×10^4 cells/ each and grown in the culture wells for 24 h prior to incubation with or without 100 μM caffeine for further 24 h. The cells were rinsed with plain medium twice and stained with 50 nM MitoTracker Red CMX Ros (Invitrogen; Eugene, OR) in serum-free medium for 30 min (at 37 °C in a humidified incubator with 5% CO_2). The nuclei were stained with Hoechst dye (Invitrogen) (1:500 in PBS) at 25 °C in the dark for 15 min. Thereafter, fixation was done by using 3.7% (v/v) formaldehyde/PBS at 25 °C in the dark for 15 min. After extensive wash with PBS, the coverslips were mounted onto the glass slides using 50% glycerol/PBS. The cells were then examined and imaged under a fluorescence microscope (Nikon; Tokyo, Japan) equipped with NIS-Elements D V.4.11 (Nikon).

In addition, quantitative analysis was done by flow cytometry. After MitoTracker staining as described above, the cells were trypsinized, resuspended in the culture medium, and analyzed by using the BD Accuri™ C6 flow cytometer (BD Biosciences). Data acquisition was done from 10,000 cells per each sample. The unstained cells served as the negative control.

2.10. Statistical analysis

All quantitative data are presented as mean ± SEM derived from three independent experiments using different biological samples. Statistical analysis between two independent groups was performed by unpaired Student's t-test, whereas differences among more than two groups were analyzed by one-way ANOVA. *P*-value < 0.05 indicates statistical significance.

3. Results

3.1. Optimal concentration of caffeine for treatment of renal tubular cells

To define the optimal concentration of caffeine to treat renal tubular cells, MDCK cells were incubated with various concentrations (0.1 – 1000 μM) of caffeine for 24 h (Fig. 1A). The optimal caffeine concentration was defined as the highest concentration that did not significantly affect total cell number and cell death (when compared with the untreated cells). The results showed that caffeine at 0.1 and 1 μM tended to increase total cell number but did not reach the statistically significant threshold. However, caffeine at 1000 μM significantly decreased the total cell number as compared with 0.1 and 1 μM (Fig. 1B). Cell death assay revealed that only 1000 μM of caffeine significantly increased the cell death (Fig. 1C). Based on these data, we therefore selected 100 μM as the optimal caffeine concentration for all subsequent experiments.

### 3.2. Caffeine-induced changes in cellular proteome of renal tubular cells

After 24-h incubation with or without 100 μM caffeine, cellular proteins were extracted and subjected to label-free quantitative proteomics using nanoLC-ESI-LTQ-Orbitrap MS/MS and MaxQuant LFQ algorithm. The MS/MS analyses identified a total of 936 proteins from these samples. Among them, 148 proteins had significantly altered levels (cutoff at ≥ 1.5-fold-change with *p*-value < 0.05) after caffeine treatment (Table 1). Some of these significantly altered proteins identified by quantitative proteomics were randomly selected for validation by Western blot analysis, which confirmed the significant decreases in levels of GAPDH, β-catenin and annexin A1 when compared with the untreated cells (Fig. 2).

3.3. Functional enrichment analysis of significantly altered proteins

All of the 148 significantly altered proteins were subjected to functional enrichment analysis to obtain their biological significance. The KEGG pathway analysis revealed that these altered proteins were involved mainly in proteasome, ribosome, tricarboxylic acid (TCA) (or Krebs) cycle, DNA replication, spliceosome, biosynthesis of amino acid, carbon metabolism, nucleocytoplasmic transport, and cell cycle (Fig. 3A). In addition, a hierarchical clustering tree has shown that the three most significant biological processes are related to cytoplasmic translation, translation initiation and mRNA metabolic process (Fig. 3B). Some of these relevant KEGG pathways and biological processes were further validated by various functional investigations as follows.

3.4. Caffeine-induced cell cycle shift in renal tubular cells

Flow cytometric analysis of the cellular DNA content was performed to determine cell cycle distribution. Comparing with the untreated control, caffeine obviously increased the cell distribution at G0/G1
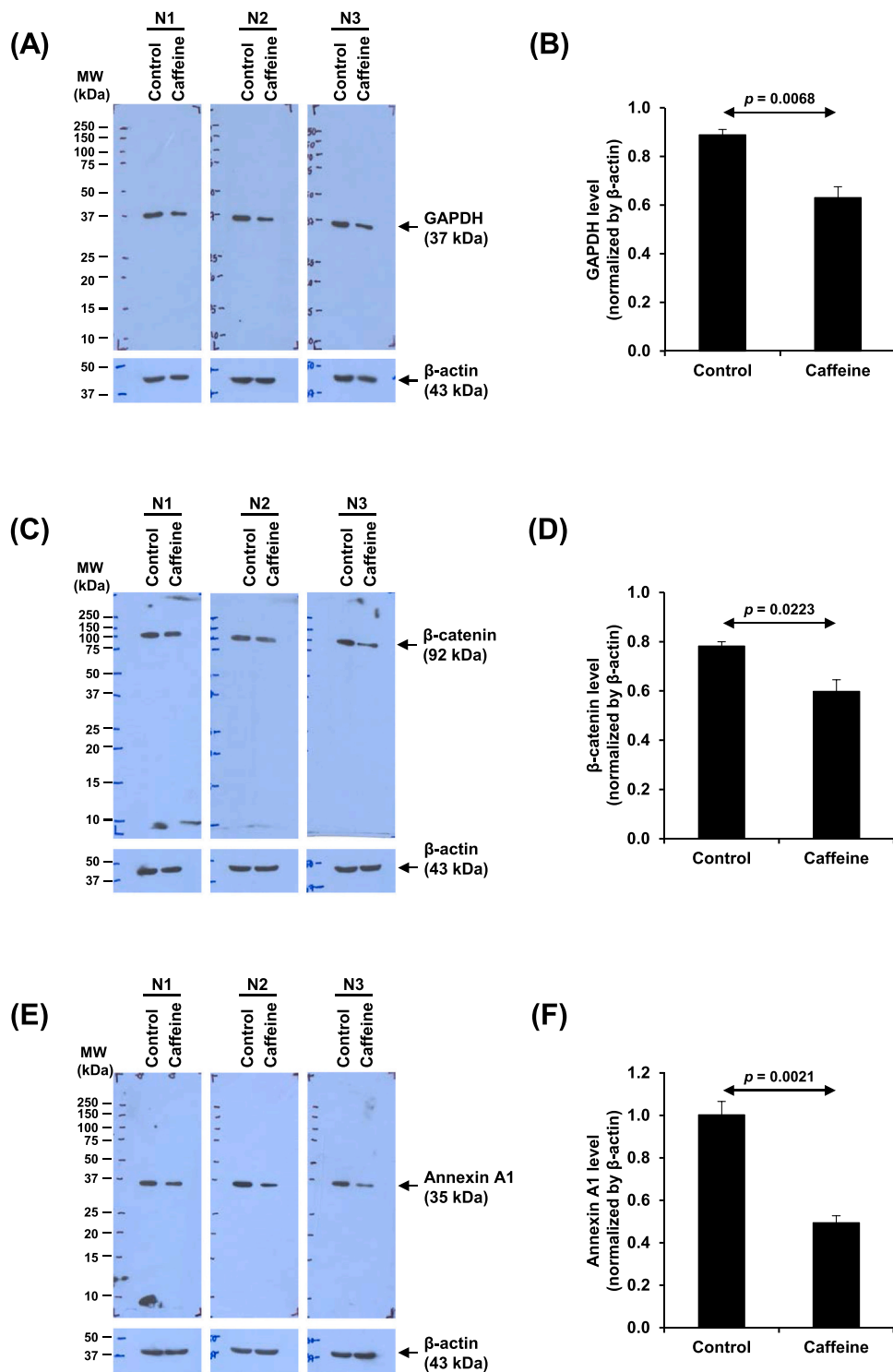
Fig. 2. Confirmation of significantly altered proteins by Western blot analyses. (A, C and E): After 24-h incubation with or without 100 μM caffeine, Western blot analyses were performed to confirm alterations in levels of GAPDH, β-catenin and annexin A1, respectively. (B, D and F): Protein band intensities were measured by using ImageQuant TL software (GE Healthcare) and normalized to that of β-actin. The data are presented as mean ± SEM derived from three independent experiments using different biological samples. Only significant *p*-values are labelled.

phase, but significantly decreased the cell distribution at G2/M phase (Fig. 4).

3.5. Caffeine-induced protein ubiquitination in renal tubular cells

The caffeine-induced modification of proteins by ubiquitination was also determined by Western blot analysis. By using an equal amount (30 μg) of total proteins loaded in each lane of SDS-PAGE, the analysis revealed that the level of ubiquitin-conjugated proteins in caffeine-treated cells was significantly greater than that in the control cells (Fig. 5).

(A) KEGG pathway

(B) Biological process
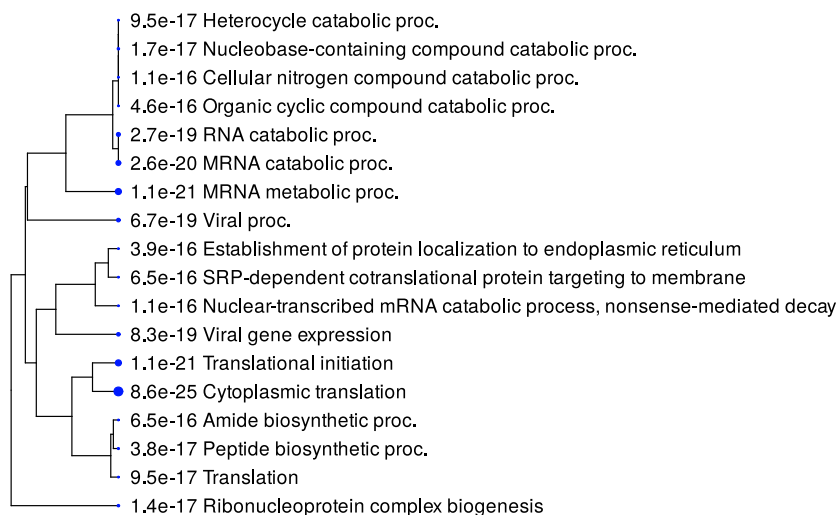
Fig. 3. Functional enrichment analysis of significantly altered proteins. All of the significantly altered proteins (cutoff at $\geq$ 1.5-fold-change with *p*-value $<$ 0.05) induced by caffeine were subjected to functional enrichment analysis using ShinyGO (version 0.77) (*http://bioinformatics.sdstate.edu/go/*). (A): The lollipop chart demonstrates the enrichment of the KEGG pathways (*https://www.genome.jp/kegg/pathway.html*). The different colors represent the different FDR-adjusted *p*-values, which were transformed into $-\log10$(FDR). (B): A hierarchical clustering tree shows the relationship among the significantly enriched biological processes. Differential sizes of the dot reflect the FDR-adjusted *p*-values, which were derived from hypergeometric distribution.

3.6. Caffeine-induced increase of intracellular ATP production in renal tubular cells

Since the TCA (Krebs) cycle was one among the enriched KEGG pathways in the significantly altered proteins induced by caffeine, intracellular ATP level was evaluated. Luminescence-based ATP measurement revealed that the intracellular ATP level was significantly increased by caffeine (Fig. 6).

3.7. Caffeine-induced increase of mitochondrial membrane potential in renal tubular cells

Finally, the cells were stained with MitoTracker Red CMX Ros to evaluate change in mitochondrial membrane potential after caffeine treatment. Immunofluorescence imaging showed the more intense fluorescence signal of the MitoTracker in the caffeine-treated cells as compared with the controls (Fig. 7A). In addition, quantitative analysis by flow cytometry revealed significantly increased fluorescence signal of the MitoTracker in the caffeine-treated cells as compared with the controls (Figs. 7B and 7C). These data indicated that caffeine caused significant increase in mitochondrial membrane potential in the renal cells.

4. Discussion

Previously, only a few studies have investigated physiological changes in the kidney and urinary tract after caffeine consumption. Using a proteomics approach, alterations in human urinary proteins are observed in healthy subjects [27]. These altered urinary proteins, i.e., kininogen, prostaglandin D2 synthase and actin, are involved mainly in

(A)

(B)
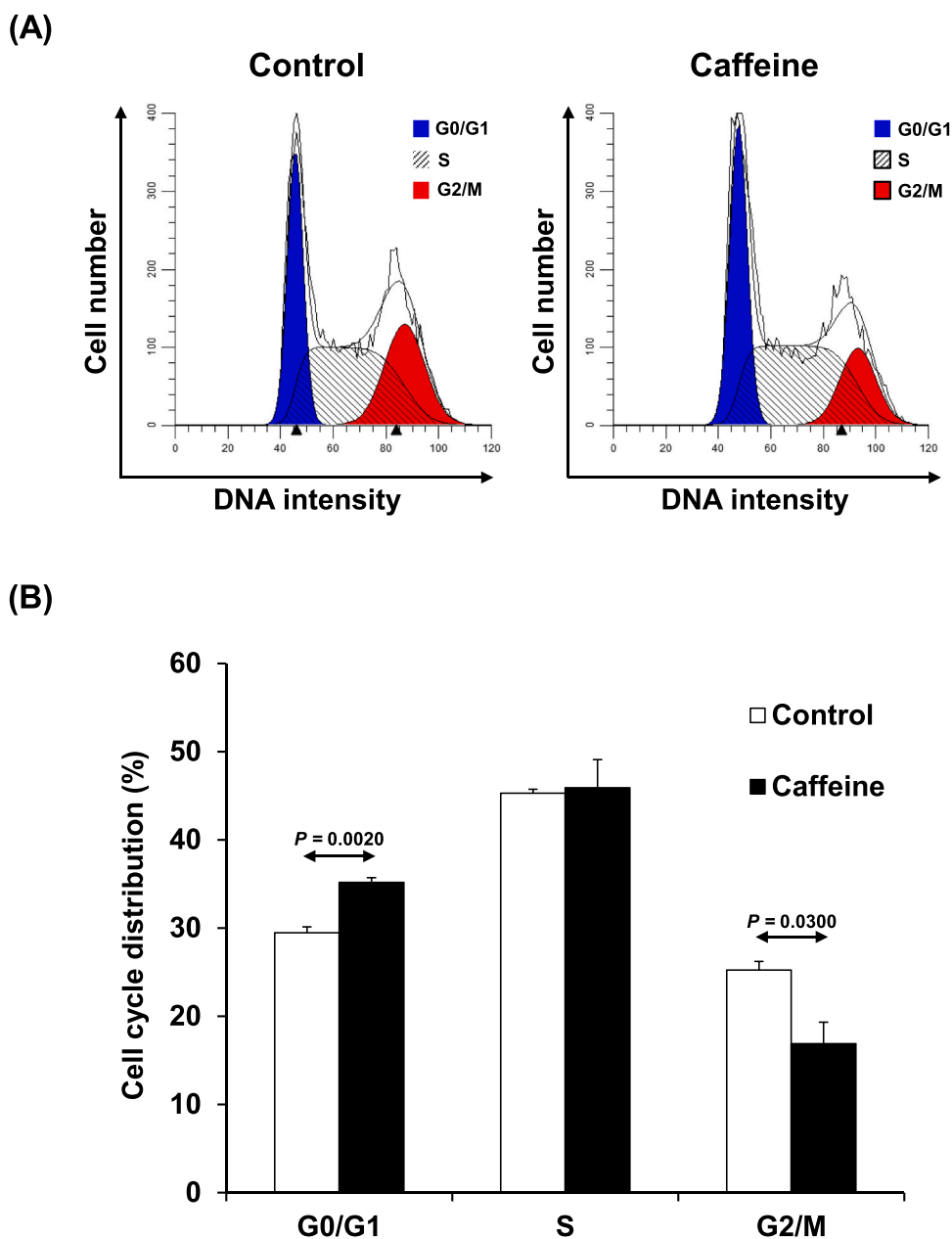
Fig. 4. Effects of caffeine on cell cycle distribution. (A): After 24-h incubation with or without 100 μM caffeine, the cells were subjected to cell cycle analysis using BD Accuri™ C6 flow cytometer (BD Biosciences). Data acquisition was done from 10,000 cells per each sample. (B): Percentage of cell population in different phases of cell cycle (G0/G1, S and G2/M) was analyzed by ModFit LT 5.0 software (Verity Software House). The data are presented as mean ± SEM derived from three independent experiments using different biological samples. Only significant *p*-values are labelled.

regulation of water balance of the whole body [27]. In addition, proteome profiling of bladder epithelial cells after caffeine treatment has shown that caffeine may trigger muscle contraction and regulation of chromatin assembly [28]. However, functional validation of the altered proteins has not been performed in these studies.

The precise cellular and molecular mechanisms underlying the effects of caffeine on the kidney remain largely unknown. This study therefore investigated the response of renal tubular cells to caffeine. The caffeine concentration employed in this study is comparable to its physiologic range in the plasma after drinking a cup of coffee [29–31]. Quantitative proteomics revealed significant changes in levels of 148 proteins involved in various KEGG pathways and biological processes. The KEGG pathway analysis showed that these significantly altered proteins were involved mainly in proteasome, ribosome, TCA (Krebs) cycle, DNA replication, spliceosome, biosynthesis of amino acid, carbon

metabolism, nucleocytoplasmic transport, and cell cycle, whereas the ShinyGO analysis demonstrated that they were involved mainly in cytoplasmic translation, translation initiation and mRNA metabolic process. According to these predicted enrichment data, functional investigations confirmed that caffeine caused cell cycle arrest at G0/G1 phase and increases of ubiquitinated proteins, intracellular ATP level, and mitochondrial membrane potential in MDCK renal cells.

To evaluate the effects of caffeine on human health, recent proteomics and muti-omics studies of cellular response of HepG2 hepatic cells to caffeine has revealed that only a small number of proteins (< 50 proteins) have significantly altered levels after caffeine treatment for 24 h even though high concentrations (100 – 1000 μM) are used [32, 33]. Herein, our data revealed a small portion of the cellular proteome of MDCK renal cells that were significantly altered by 100 μM caffeine treatment for 24 h, suggesting that the condition used herein did not

(A)

(B)
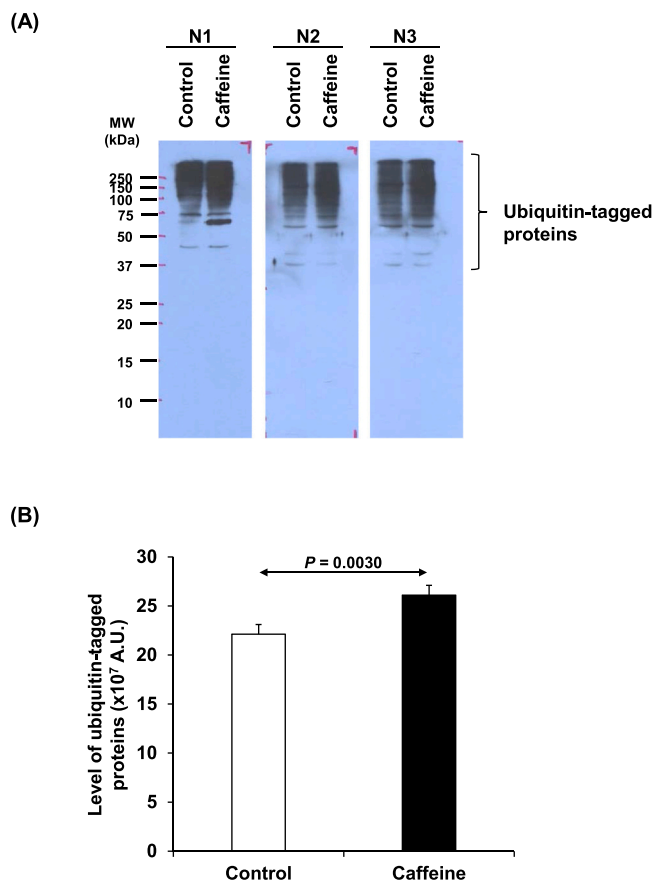
Fig. 5. Effects of caffeine on protein ubiquitination. (A): After 24-h incubation with or without 100 μM caffeine, Western blot analysis was performed to measure level of ubiquitin-conjugated proteins. (B): Intensities of multiple protein bands in each lane were measured by using ImageQuant TL software (GE Healthcare). The data are presented as mean ± SEM derived from three independent experiments using different biological samples. A.U. = arbitrary unit.
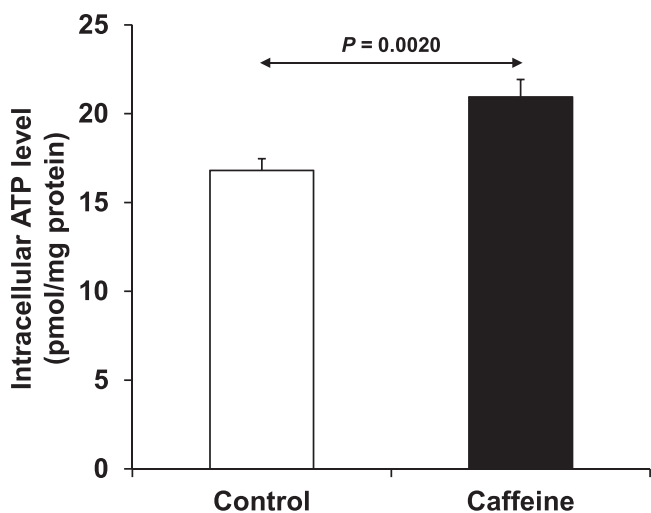

Fig. 6. Effects of caffeine on intracellular ATP level. After 24-h incubation with or without 100 μM caffeine, the intracellular ATP level was measured by a luminescence-based assay based on the standard curve and normalized by the protein amount. The data are presented as mean ± SEM (in pmol/mg protein unit) derived from three independent experiments using different biological samples.

induce obvious cytotoxic effects, but rather reflected the cellular adaptive response of the renal cells to caffeine. In addition, our findings were consistent with the findings reported from previous studies showing that caffeine commonly affects ribosome and cytoplasmic translation of HepG2 hepatocytes [32] and EA.hy926 endothelial cells [34,35], implicating that caffeine regulates cytoplasmic translation and mRNA metabolic process.

It is well-known that caffeine can induce cell cycle arrest in many cancer cells in vitro. For instance, caffeine increases cell population at G0/G1 (G0/G1 phase arrest) but decreases S phase population of glioblastoma cells, resulting in an inhibition of cell proliferation [36]. Caffeine can also suppress proliferation of lung carcinoma cells by causing G0/G1 phase arrest and inhibiting cell migration/invasion by altering the pattern of integrins and FAK/Akt/c-Myc signaling axis [37]. Caffeine also causes G0/G1 phase arrest by reducing phosphorylation of pRb, thereby suppressing activation of cyclin D1/cdk 4 complex [38]. Additionally, caffeine can regulate cell cycle by p53-dependent and p53-independent mechanisms [39]. In consistent with the previous studies, our results showed that the cell distribution at G0/G1 phase was increased, whereas the G2/M phase population was decreased by caffeine. These data suggested that caffeine could induce G0/G1 phase arrest in renal tubular cells. Interestingly, a recent in vitro model of renal tubular cell injury has shown that, after the injury, the repairing cells have cell cycle shift from G0/G1 to S and G2/M phases during the repair process [40]. Moreover, such cell cycle shift induced by scratch and by chemicals (hydroxyurea and cyclosporin A) at sub-toxic concentrations enhances calcium oxalate (CaOx) crystal adhesion on renal tubular cell surface that is one of the initial processes of kidney stone formation. Therefore, the reverse effect of cell cycle shift by caffeine shown in our present study may be the renoprotective mechanism to prevent CaOx crystal adhesion at renal tubular cell surface.

In addition to the cell cycle shift, we confirmed the decreased expression of annexin A1 in renal tubular cells after caffeine treatment. Annexin A1 has been identified as one of the CaOx crystal receptors and plays significant roles in crystal-cell adhesion [41,42]. Therefore, such decrease of this CaOx crystal receptor may be another renoprotective mechanism to prevent CaOx crystal adhesion at renal tubular cell surface. The present data are in agreement with the findings in our previous report demonstrating that caffeine also reduces apical surface expression of annexin A1 by translocating its surface form to cytoplasm, leading to suppression of CaOx crystal-cell adhesion [43]. Such translocation is most likely due to the decreased intracellular storage of calcium as caffeine can induce secretion of calcium ions from the cells [43]. The influence of low-calcium concentration on annexin A1 translocation from apical surface to cytoplasm has been confirmed by experimental evidence [43]. These data suggest the roles of caffeine in kidney stone prevention.

Interestingly, caffeine can affect proteasome activity. A previous in vitro study of UV-induced translesion replication in murine fibroblasts has demonstrated that caffeine suppresses this process and affects cell death after UV radiation [44]. The mechanism underlying this phenomenon has been proposed to be mediated by inhibiting proteasome 26 S activity because the findings are similar to those induced by a proteasome inhibitor (MG-262) [44]. In addition, caffeine can suppress lipid accumulation in adipocytes by mitigating inflammatory cytokines produced by intestinal epithelial cells [45]. The responsible mechanism is related to the ability of caffeine to target peroxisome proliferator-activated receptor γ (PPARγ) and CCAAT/enhancer binding protein α (C/EBPα) in adipocytes for degradation via ubiquitin-proteasome pathway [45]. In general, the increase in ubiquitin-conjugated proteins commonly occurs and is necessary for the cells to reestablish hemostasis after an adaptive response to mild oxidative stress [46]. Mild oxidative stress can induce the rate of protein ubiquitination by enhancing the activity of ubiquitin-conjugating enzymes and increasing their substrates [46]. On the other hand, sustained or severe oxidative stress can lead to a dramatic decrease in the ubiquitin
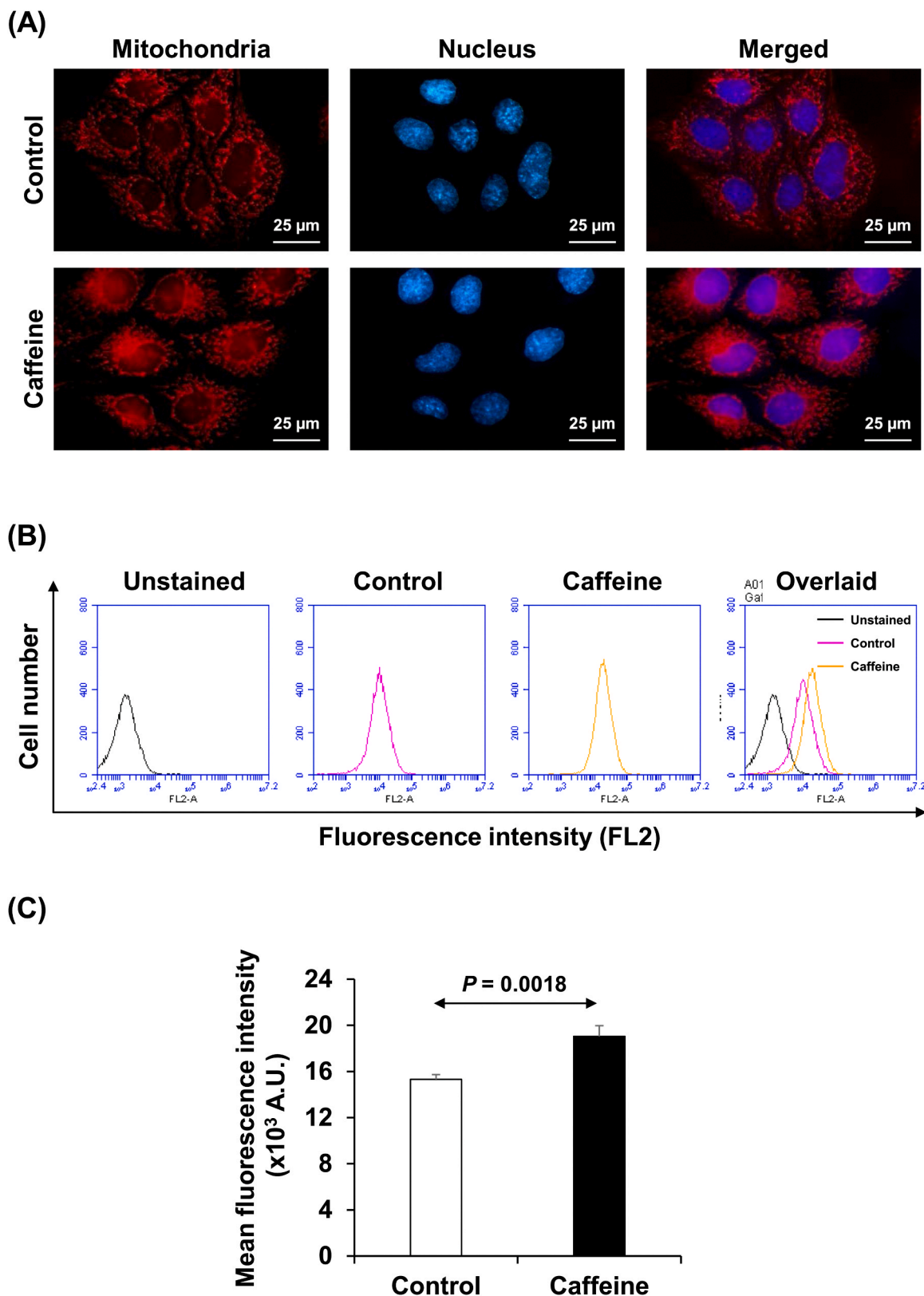
Fig. 7. Effects of caffeine on mitochondrial membrane potential. (A): After 24-h incubation with or without 100 μM caffeine, mitochondrial membrane potential was determined by staining with MitoTracker Red CMX Ros (Invitrogen). The cells were then examined and imaged under a fluorescence microscope (Nikon). (B): Histogram of fluorescence intensity of the MitoTracker analyzed by the BD Accuri™ C6 flow cytometer (BD Biosciences). The unstained cells served as the negative control. (C): The data were quantified from 10,000 cells per each sample. The quantitative data are presented as mean ± SEM derived from three independent experiments using different biological samples. A.U. = arbitrary unit.

conjugates due to the decline activities of ubiquitin-conjugating enzymes and impaired proteasome [46]. Additionally, both mild and severe oxidative stresses can inactivate the 26 S proteasome [47]. In the present study, our results showed the increased level of ubiquitin-conjugated proteins, implicating that caffeine might inhibit proteasome activity of renal tubular cells. Although the precise mechanism remains unclear, an opportunity arises for the investigation of these target proteins and their involvement in the cellular response of the renal cells to caffeine.

In consistent with our present study, a previous study combining proteomics and metabolomics approaches has revealed that coffee consumption may result in an increase of energy production as indicated by the upregulated isocitrate dehydrogenase, a major enzyme involved in TCA (Krebs) cycle, and the increases of urea cycle metabolites [48]. Specific micronutrients, including caffeine, can restore mitochondrial functions by boosting electron transport complexes (i.e., complexes I and IV), thereby increasing ATP production and improving illness convalescence [49]. Additionally, intracellular ATP level is involved in the homeostasis of mitochondrial membrane potential ($\Delta\Psi$m) – the greater ATP level, the more stability of the membrane potential [50]. The $\Delta\Psi$m is necessary not only for ATP synthesis but also for mitochondrial protein transport and retrograde signaling (mitochondria-to-nucleus communication) [51,52]. Herein, we also observed the increased intracellular ATP level and the elevated mitochondrial membrane potential after caffeine treatment. These findings support that caffeine plays regulatory roles in enhancing energy generation and energy outflow, which are imperative for mitochondrial quality control and cell survival.

In summary, this study has revealed the potential of quantitative proteomics to gain insights into cellular adaptive response of renal tubular cells to caffeine at the protein level. Functional enrichment analysis has shown that caffeine affects many KEGG pathways (particularly proteasome, ribosome, TCA (Krebs) cycle, DNA replication, spliceosome, biosynthesis of amino acid, carbon metabolism, nucleocytoplasmic transport and cell cycle) and biological processes (particularly cytoplasmic translation, translation initiation and mRNA metabolic process). Functional validation by various assays confirms that caffein causes cell cycle arrest at G0/G1 and increases of ubiquitinated proteins, intracellular ATP and mitochondrial membrane potential in MDCK cells. These data may help unravelling cellular and molecular mechanisms underlying the biological effects of caffeine on the renal cells. It should be noted that the cells were treated by a physiologic concentration of caffeine for only 24 h. Changes in the cellular proteome and other elements may differ if the treatment is prolonged. Therefore, further proteomics and multi-omics studies of serial changes in cellular proteome and other elements at various time-points should be performed to enhance this knowledge.

CRediT authorship contribution statement

RK and VT designed research; RK, CS and SN performed experiments; RK, CS, SN and VT analyzed data; RK and VT wrote the manuscript; All authors reviewed and approved the manuscript.

Declaration of Competing Interest

The authors declare that they have no known competing financial interests or personal relationships that could have appeared to influence the work reported in this paper.

Data availability

All data generated or analyzed during this study are included in this published article. In addition, the mass spectrometry proteomics data have been deposited to the ProteomeXchange Consortium (*http://www. proteomexchange.org/*) via the PRIDE (*https://www.ebi.ac.uk/pride/*)

partner repository with the dataset identifier PXD045313 and 10.6019/ PXD045313. (Username: reviewer_pxd045313 @ebi.ac.uk/ Pass: fSdRLflx).

References

[1] Monjotin N, Amiot MJ, Fleurentin J, Morel JM, Raynal S. Clinical evidence of the benefits of phytonutrients in human healthcare. Nutrients 2022;14:1712.

[2] Reyes CM, Cornelis MC. Caffeine in the diet: country-level consumption and guidelines. Nutrients 2018;10:1772.

[3] Asadi-Pooya AA, Zeraatpisheh Z, Rostaminejad M, Damabi NM. Caffeinated drinks, fruit juices, and epilepsy: a systematic review. Acta Neurol Scand 2022;145: 127–38.

[4] Nehlig A. Interindividual differences in caffeine metabolism and factors driving caffeine consumption. Pharmacol Rev 2018;70:384–411.

[5] Rodak K, Kokot I, Kratz EM. Caffeine as a factor influencing the functioning of the human body-friend or foe. Nutrients 2021;13:3088.

[6] O'Keefe JH, DiNicolantonio JJ, Lavie CJ. Coffee for cardioprotection and longevity. Prog Cardiovasc Dis 2018;61:38–42.

[7] Miranda-Diaz AG, Garcia-Sanchez A, Cardona-Munoz EG. Foods with potential prooxidant and antioxidant effects involved in parkinson's disease. Oxid Med Cell Longev 2020;2020:6281454.

[8] Kanbay M, Siriopol D, Copur S, Tapoi L, Benchea L, Kuwabara M, et al. Effect of coffee consumption on renal outcome: a systematic review and meta-analysis of clinical studies. J Ren Nutr 2021;31:5–20.

[9] Li Y, Li W, Lu Y, Zhang J. Coffee consumption is associated with a decreased risk of incident chronic kidney disease: a protocol for systematic review and meta-analysis. Med Baltim 2021;100:e27149.

[10] Srithongkul T, Ungprasert P. Coffee consumption is associated with a decreased risk of incident chronic kidney disease: a systematic review and meta-analysis of cohort studies. Eur J Intern Med 2020;77:111–6.

[11] Peerapen P, Thongboonkerd V. Caffeine in kidney stone disease: risk or benefit. Adv Nutr 2018;9:419–24.

[12] Barghouthy Y, Corrales M, Doizi S, Somani BK, Traxer O. Tea and coffee consumption and pathophysiology related to kidney stone formation: a systematic review. World J Urol 2021;39:2417–26.

[13] Geng J, Qiu Y, Kang Z, Li Y, Li J, Liao R, et al. The association between caffeine intake and risk of kidney stones: a population-based study. Front Nutr 2022;9: 935820.

[14] Zhao J, Huang Y, Yu X. Caffeine intake and the risk of incident kidney stones: a systematic review and meta-analysis. Int Urol Nephrol 2022;54:2457–66.

[15] Yuan S, Larsson SC. Coffee and caffeine consumption and risk of kidney stones: a mendelian randomization study. Am J Kidney Dis 2022;79:9–14. e1.

[16] Massey LK, Sutton RA. Acute caffeine effects on urine composition and calcium kidney stone risk in calcium stone formers. J Urol 2004;172:555–8.

[17] Fenton RA, Poulsen SB, de la Mora Chavez S, Soleimani M, Busslinger M, Dominguez Rieg JA, et al. Caffeine-induced diuresis and natriuresis is independent of renal tubular nhe3. Am J Physiol Ren Physiol 2015;308:F1409–20.

[18] Chaiyarit S, Thongboonkerd V. Oxidized forms of uromodulin promote calcium oxalate crystallization and growth, but not aggregation. Int J Biol Macromol 2022; 214:542–53.

[19] Chaiyarit S, Thongboonkerd V. Oxidative modifications switch modulatory activities of urinary proteins from inhibiting to promoting calcium oxalate crystallization, growth, and aggregation. Mol Cell Proteom 2021;20:100151.

[20] Yoodee S, Noonin C, Sueksakit K, Kanlaya R, Chaiyarit S, Peerapen P, et al. Effects of secretome derived from macrophages exposed to calcium oxalate crystals on renal fibroblast activation. Commun Biol 2021;4:959.

[21] Wuttimongkolchai N, Kanlaya R, Nanthawuttiphan S, Subkod C, Thongboonkerd V. Chlorogenic acid enhances endothelial barrier function and promotes endothelial tube formation: a proteomics approach and functional validation. Biomed Pharm 2022;153:113471.

[22] Tyanova S, Temu T, Cox J. The maxquant computational platform for mass spectrometry-based shotgun proteomics. Nat Protoc 2016;11:2301–19.

[23] Kanlaya R, Kapincharanon C, Fong-Ngern K, Thongboonkerd V. Induction of mesenchymal-epithelial transition (met) by epigallocatechin-3-gallate to reverse epithelial-mesenchymal transition (emt) in snai1-overexpressed renal cells: a potential anti-fibrotic strategy. J Nutr Biochem 2022;107:109066.

[24] Fong-ngern K, Ausakunpipat N, Singhto N, Sueksakit K, Thongboonkerd V. Prolonged k(+) deficiency increases intracellular atp, cell cycle arrest and cell death in renal tubular cells. Metabolism 2017;74:47–61.

[25] Sutthimethakorn S, Thongboonkerd V. Effects of high-dose uric acid on cellular proteome, intracellular atp, tissue repairing capability and calcium oxalate crystal-binding capability of renal tubular cells: implications to hyperuricosuria-induced kidney stone disease. Chem Biol Inter 2020;331:109270.

[26] Gallemit PEM, Yoodee S, Malaitad T, Thongboonkerd V. Epigallocatechin-3-gallate plays more predominant roles than caffeine for inducing actin-crosslinking, ubiquitin/proteasome activity and glycolysis, and suppressing angiogenesis features of human endothelial cells. Biomed Pharm 2021;141:111837.

[27] Peerapen P, Ausakunpipat N, Sutthimethakorn S, Aluksanasuwan S, Vinaiphat A, Thongboonkerd V. Physiologic changes of urinary proteome by caffeine and excessive water intake. Clin Chem Lab Med 2017;55:993–1002.

[28] Shahid M, Kim M, Yeon A, Andres AM, You S, Kim J. Quantitative proteomic analysis reveals caffeine-perturbed proteomic profiles in normal bladder epithelial cells. Proteomics 2018;18:e1800190.

[29] Teekachunhatean S, Tosri N, Rojanasthien N, Srichairatanakool S, Sangdee C. Pharmacokinetics of caffeine following a single administration of coffee enema versus oral coffee consumption in healthy male subjects. ISRN Pharmacol 2013; 2013:147238.

[30] Skinner TL, Jenkins DG, Leveritt MD, McGorm A, Bolam KA, Coombes JS, et al. Factors influencing serum caffeine concentrations following caffeine ingestion. J Sci Med Sport 2014;17:516–20.

[31] Spriet LL. Exercise and sport performance with low doses of caffeine. Sports Med 2014;44(Suppl 2):S175–84.

[32] Peerapen P, Chanthick C, Thongboonkerd V. Quantitative proteomics reveals common and unique molecular mechanisms underlying beneficial effects of caffeine and trigonelline on human hepatocytes. Biomed Pharm 2023;158:114124.

[33] Li Y, Zhang Z, Jiang S, Xu F, Tulum L, Li K, et al. Using transcriptomics, proteomics and phosphoproteomics as new approach methodology (nam) to define biological responses for chemical safety assessment. Chemosphere 2023;313:137359.

[34] Chanthick C, Thongboonkerd V. Comparative proteomics reveals concordant and discordant biochemical effects of caffeine versus epigallocatechin-3-gallate in human endothelial cells. Toxicol Appl Pharmacol 2019;378:114621.

[35] Chanthick C, Thongboonkerd V. Cellular proteome datasets of human endothelial cells under physiologic state and after treatment with caffeine and epigallocatechin-3-gallate. Data Brief 2019;25:104292.

[36] Jiang J, Lan YQ, Zhang T, Yu M, Liu XY, Li LH, et al. The in vitro effects of caffeine on viability, cycle cycle profiles, proliferation, and apoptosis of glioblastomas. Eur Rev Med Pharmacol Sci 2015;19:3201–7.

[37] Meisaprow P, Aksorn N, Vinayanuwattikun C, Chanvorachote P, Sukprasansap M. Caffeine induces g0/g1 cell cycle arrest and inhibits migration through integrin alphav, beta3, and fak/akt/c-myc signaling pathway. Molecules 2021;26:7659.

[38] Hashimoto T, He Z, Ma WY, Schmid PC, Bode AM, Yang CS, et al. Caffeine inhibits cell proliferation by g0/g1 phase arrest in jb6 cells. Cancer Res 2004;64:3344–9.

[39] Cui WQ, Wang ST, Pan D, Chang B, Sang LX. Caffeine and its main targets of colorectal cancer. World J Gastrointest Oncol 2020;12:149–72.

[40] Khamchun S, Thongboonkerd V. Cell cycle shift from g0/g1 to s and g2/m phases is responsible for increased adhesion of calcium oxalate crystals on repairing renal tubular cells at injured site. Cell Death Discov 2018;4:106.

[41] Fong-ngern K, Peerapen P, Sinchaikul S, Chen ST, Thongboonkerd V. Large-scale identification of calcium oxalate monohydrate crystal-binding proteins on apical membrane of distal renal tubular epithelial cells. J Proteome Res 2011;10: 4463–77.

[42] Chutipongtanate S, Fong-ngern K, Peerapen P, Thongboonkerd V. High calcium enhances calcium oxalate crystal binding capacity of renal tubular cells via increased surface annexin a1 but impairs their proliferation and healing. J Proteome Res 2012;11:3650–63.

[43] Peerapen P, Thongboonkerd V. Caffeine prevents kidney stone formation by translocation of apical surface annexin a1 crystal-binding protein into cytoplasm: in vitro evidence. Sci Rep 2016;6:38536.

[44] Takezawa J, Aiba N, Kajiwara K, Yamada K. Caffeine abolishes the ultraviolet-induced rev3 translesion replication pathway in mouse cells. Int J Mol Sci 2011;12: 8513–29.

[45] Mitani T, Nagano T, Harada K, Yamashita Y, Ashida H. Caffeine-stimulated intestinal epithelial cells suppress lipid accumulation in adipocytes. J Nutr Sci Vitam 2017;63:331–8.

[46] Shang F, Taylor A. Ubiquitin-proteasome pathway and cellular responses to oxidative stress. Free Radic Biol Med 2011;51:5–16.

[47] Reeg S, Castro JP, Hugo M, Grune T. Accumulation of polyubiquitinated proteins: a consequence of early inactivation of the 26s proteasome. Free Radic Biol Med 2020;160:293–302.

[48] Takahashi S, Saito K, Jia H, Kato H. An integrated multi-omics study revealed metabolic alterations underlying the effects of coffee consumption. PLoS One 2014; 9:e91134.

[49] Wesselink E, Koekkoek WAC, Grefte S, Witkamp RF, van Zanten ARH. Feeding mitochondria: potential role of nutritional components to improve critical illness convalescence. Clin Nutr 2019;38:982–95.

[50] Zorova LD, Popkov VA, Plotnikov EY, Silachev DN, Pevzner IB, Jankauskas SS, et al. Mitochondrial membrane potential. Anal Biochem 2018;552:50–9.

[51] Sato TK, Kawano S, Endo T. Role of the membrane potential in mitochondrial protein unfolding and import. Sci Rep 2019;9:7637.

[52] Kulawiak B, Hopker J, Gebert M, Guiard B, Wiedemann N, Gebert N. The mitochondrial protein import machinery has multiple connections to the respiratory chain. Biochim Biophys Acta 2013;1827:612–26.